Probing vertically graded anisotropy in FePtCu films

Randy K. Dumas,[1,*] Yeyu Fang,[2] B. J. Kirby,[3] Chaolin Zha,[2] Valentina Bonanni,[2] Josep Nogués,[2,4] and Johan Åkerman[1,2]

[1]*Department of Physics, University of Gothenburg, Gothenburg 412 96, Sweden*
[2]*Materials Physics, Royal Institute of Technology (KTH), Kista 164 40, Sweden*
[3]*Center for Neutron Research, National Institute of Standards and Technology, Gaithersburg, Maryland 20899, USA*
[4]*Institució Catalana de Recerca i Estudis Avançats (ICREA) and CIN2 (ICN-CSIC) and Universitat Autònoma de Barcelona,*
Catalan Institute of Nanotechnology, Campus de la Universitat Autònoma de Barcelona, Bellaterra (Barcelona) 08193, Spain

Field-dependent polarized neutron reflectivity (PNR) and magnetometry are employed to study the magnetic properties of compositionally uniform and graded FePtCu films as a function of annealing temperature (T_A). The PNR results are able to directly probe the compositional and anisotropy variations through the film thickness. Further details about how the reversal mechanisms evolve are then elucidated by using a first-order reversal curve technique. The reversal of the graded sample annealed at 300 °C occurs by an initial rapid switching of the dominant soft A1 phase toward the surface of the film, followed by the gradual reversal of the residual hard phase components toward the bottom. This indicates that the anisotropy gradient is not well established at this low T_A. A fundamentally different mechanism is found after annealing at 400 °C, where the rapid switching of the entire film is preceded by a gradual reversal of the soft layers. This suggests that the anisotropy gradient has become better established through the film thickness. The field-dependent PNR measurements confirm the existence of an anisotropy gradient, where the lower (higher) anisotropy portions are now toward the bottom (top) of the film because of the Cu compositional gradient. However, after annealing at 500 °C, a single rapid reversal is found, indicating the formation of a uniform hard film. In this case, PNR demonstrates a more uniform magnetic depth profile that is consistent with a uniform reference sample, suggesting significant interdiffusion of the Cu is degrading the compositional and induced anisotropy gradient at this elevated T_A.

I. INTRODUCTION

The study of magnetically heterogeneous systems is a primary focal point of intense research because of their fascinating physical properties and immediate applicability. In particular, binary systems based on ferromagnet (FM)/antiferromagnet (AFM)[1] and high anisotropy-FM/low anisotropy-FM[2,3] layered and nanocomposite materials have garnered the most interest to date. However, graded anisotropy systems,[4,5] where the anisotropy is continuously varied through the film thickness, are currently being aggressively pursued. Graded anisotropy materials have been primarily motivated by their potential use as magnetic recording media. They join tilted[6,7] and exchange coupled composite (ECC) media,[8] as well as heat-assisted magnetic recording[9] and microwave-assisted magnetic recording[10] techniques as possible solutions to the magnetic recording "trilemma."[11,12] Successful, long-term storage relies on simultaneously balancing the *thermal stability, signal-to-noise ratio,* and *writability* of a given bit. To achieve areal bit densities of in excess of 1 Tbit/in^2, the volume of the constituent grains approaches the point where thermal fluctuations begin to dominate as the grains become superparamagnetic. Although high anisotropy materials dramatically improve thermal stability, the magnetic fields required for switching far exceed the capabilities of the write head. Graded anisotropy media is predicted to provide additional gains in writability[4,13] over conventional bilayer hard/soft ECC media in that the low anisotropy layers act to reduce the switching field while the thermal stability is maintained by the high anisotropy layers. Fabrication schemes to realize graded films remain few and have mostly relied on multilayered approaches.[14–19]

However, a continuous anisotropy gradient has been recently realized in properly annealed, compositionally graded FePtCu films.[20,21] In addition, similar FePtCu films have been shown to have a tilted anisotropy[22,23] that, when combined with the advantages of graded anisotropy, may result in versatile material suitable for both magnetic recording and spin transfer torque applications.[24,25] Finally, in addition to fabrication challenges, direct experimental verification of an anisotropy gradient is experimentally challenging. Although the inherent depth sensitivity of polarized neutron reflectivity (PNR) measurements[17,18] have recently been used to directly probe the anisotropy gradient, most experimental works on graded anisotropy films have primarily focused on analysis of the switching field and/or improved thermal stability to indirectly infer the anisotropy gradient.

In this paper, we combine PNR measurements—to directly probe the compositional and anisotropy variations through the film thickness—with the first-order reversal curve (FORC)[21,26–31] technique to provide a comprehensive study of how the anisotropy gradient evolves as a function of annealing temperature (T_A) in both compositionally uniform and graded films. In addition to providing a useful qualitative "fingerprint" of the magnetization reversal mechanisms, FORC analysis has shown the ability to extract a wealth of quantitative information in a variety of bulk,[32] thin film,[26,27,33,34] and patterned[28,30,31,35,36] material systems that are not readily accessible from standard major loop or remanence curve analysis. As the T_A is increased, distinct changes in the magnetic depth profiles and FORC "fingerprints" are observed. The PNR analysis of the compositionally graded sample annealed at 300 °C indicates that anisotropy increases with

proximity to the film/substrate interface, consistent with more rapid formation of the $L1_0$ phase toward the bottom, Cu-rich region. However, when the T_A is increased to $400\,^\circ\text{C}$, a fundamentally different reversal mechanism is revealed, where the rapid switching of the entire film is initiated by the gradual reversal of the soft layers. Here, the PNR results suggest a reversed anisotropy gradient, where the bottom of the film is now relatively softer. This is consistent with a better-established anisotropy gradient throughout the film thickness because of an elevated T_A, and the Cu concentration gradient, which now acts to soften the bottom regions compared to the surface. Finally, after annealing at $500\,^\circ\text{C}$, a single rapid reversal process, with only a residual hard phase component, is observed, because significant interdiffusion of the Cu at this elevated T_A results in a compositionally uniform film that is virtually indistinguishable from the compositionally uniform reference sample.

II. EXPERIMENT

Both the compositionally uniform and the graded samples were deposited at room temperature on thermally oxidized Si substrates by magnetron sputtering of high purity Fe, Pt, and Cu targets in a chamber with a base pressure better than 6×10^{-6} Pa. To improve surface roughness, (111) texture, and to lower the chemical ordering temperature of the $L1_0$ phase, the FePtCu films were deposited on a bilayer of Ta (6 nm)/Pt (3 nm)[37] and capped with 5 nm of Ta to prevent oxidation. To achieve a compositional gradient through the sample thickness, the sputtering power of the Cu gun was continuously varied from 35 to 0 W. The resulting 20-nm-thick $(\text{Fe}_{53}\text{Pt}_{47})_{100-x}\text{Cu}_x$ ($x = 0$–30) film (referred to as graded FePtCu) is Cu-rich $(\text{Fe}_{53}\text{Pt}_{47})_{70}\text{Cu}_{30}$ at the bottom and Cu-free $\text{Fe}_{53}\text{Pt}_{47}$ at the top. As a reference, a compositionally uniform sample (referred to as uniform FePtCu) with the same total Cu content as the graded sample, $(\text{Fe}_{53}\text{Pt}_{47})_{85}\text{Cu}_{15}$, was also deposited. The strong dependence of the A1 (low anisotropy) $\rightarrow$ $L1_0$ (high anisotropy) ordering temperature on the Cu content[38] is then used to generate an anisotropy gradient in the compositionally graded film. The Cu-rich regions toward the bottom are expected to transform from the as-deposited low anisotropy cubic A1 phase into the high anisotropy tetragonal $L1_0$ phase at a lower T_A than the Cu-poor regions toward the top, thus establishing the anisotropy gradient. Separate pieces of the graded and uniform FePtCu films were then annealed at $T_A = 300\,^\circ\text{C}$, $400\,^\circ\text{C}$, and $500\,^\circ\text{C}$ for 35 min in vacuum. For additional details on sample fabrication and more detailed structural characterization, e.g., x-ray diffraction, see Ref. [20].

Room-temperature, field-dependent PNR measurements on the compositionally graded and uniform FePtCu films were conducted using the NG1 Reflectometer at the National Institute of Standards and Technology's Center for Neutron Research. A 0.475-nm cold neutron beam was polarized to be spin-up or spin-down relative to an applied magnetic field and was incident on a given sample. The spin-dependent specular reflectivities were measured as functions of the wavevector transfer along the surface normal (Q_z). No significant spin-flip scattering (which arises from the in-plane component of the sample magnetization perpendicular to the applied field) was

detected for any sample under any condition; thus, we refer only to the spin-down $(-)$ and spin-up $(+)$ non-spin-flip reflectivities.

The reversal mechanisms have been measured using standard magnetometry with an alternating gradient magnetometer (AGM) at room temperature and with the field applied parallel to the film plane. In addition to standard major loop measurements, the AGM is used to measure families of FORCs using the following procedure. After positive saturation, the applied field is reduced to a given reversal field H_R. From this reversal field, the magnetization is then measured back toward positive saturation, thereby tracing out a single FORC. This process is repeated for a series of decreasing reversal fields, thus filling the interior of the major hysteresis loop, which can be seen as the outer boundary of the family of FORCs. The FORC distribution is then defined as a mixed second-order derivative of the normalized magnetization,

$$\rho(H, H_R) \equiv -\frac{1}{2}\frac{\partial^2 M(H, H_R)/M_S}{\partial H \partial H_R}, \tag{1}$$

which is then plotted against (H, H_R) coordinates on a contour map. For a given H_R, the magnetization is measured for increasing applied fields H; therefore, $H \geqslant H_R$ by design. Following the measurement procedure, the FORC distribution is read in a "top-down" fashion and from left to right for a particular reversal field. The FORC distribution provides a useful fingerprint of the reversal mechanism by mapping out, in (H, H_R) coordinates, only the *irreversible* switching processes. It is often useful to have a one-dimensional visualization of the irreversibility by projecting the FORC distribution onto the H_R axis. This is equivalent to an integration over the applied field H,

$$\int \frac{\partial^2 M(H, H_R)}{\partial H \partial H_R}dH = \frac{\partial M(H_R)}{\partial H_R}, \tag{2}$$

and is termed a FORC–switching field distribution (FORC-SFD). This can then be easily compared with the standard technique of taking the derivative of the dc-demagnetization (DCD) curve to determine the DCD–switching field distribution (DCD-SFD):

$$\frac{\partial M_r(H_R)}{\partial H_R}. \tag{3}$$

Here $M_r(H_R)$ is the zero-field magnetization, or remanence, after the application of a given reversal field H_R. The DCD-SFD data can be conveniently extracted from the measured family of FORCs as the remanent state is measured for each reversal curve. For direct comparison, both the FORC-SFD and the DCD-SFD are normalized by their maximum value. Although the DCD-SFD and FORC-SFD are similar, they are sensitive to different aspects of the reversal. The DCD-SFD only probes switching processes as manifested at the remanent state, whereas the FORC-SFD accounts for *irreversibility* along the *entire* reversal curve.

III. RESULTS AND DISCUSSIONS

The inherent sensitivity to the nuclear and magnetic depth profiles[39,40] makes PNR an ideal probe for graded anisotropy thin films.[17,18] PNR measurements demonstrate strong
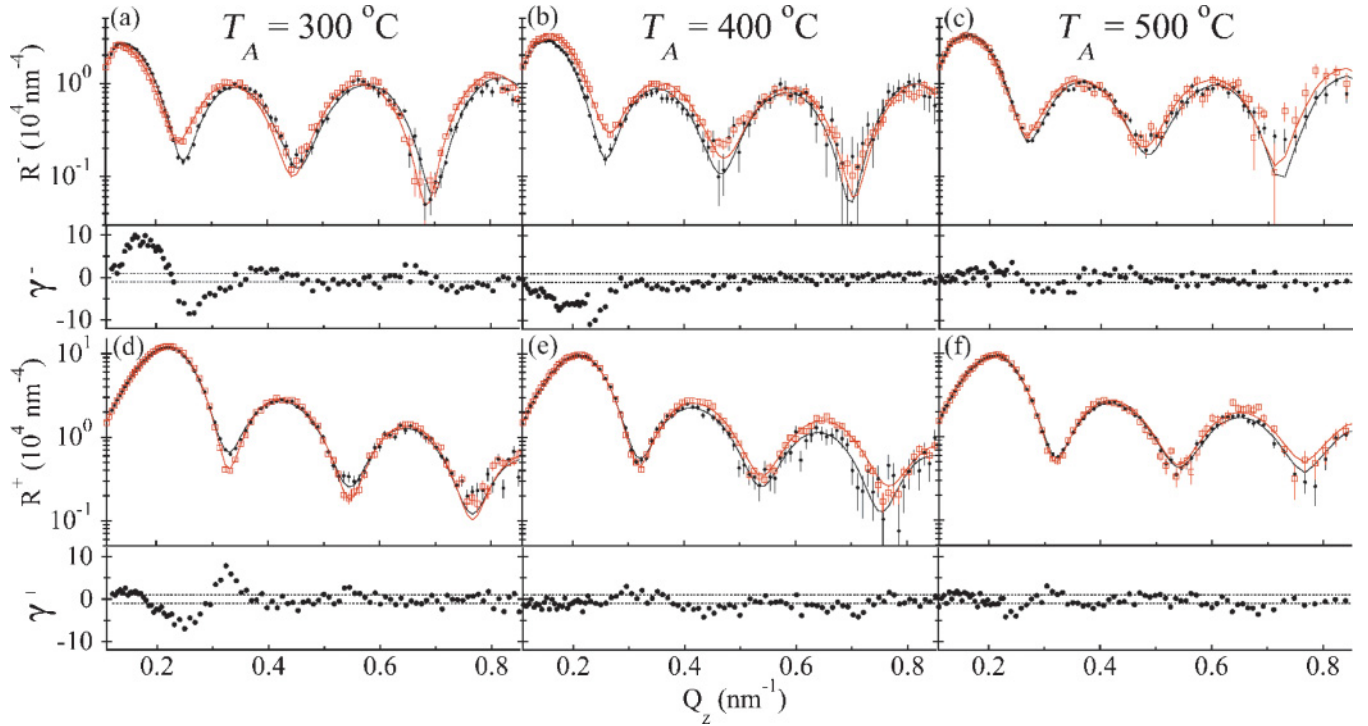
FIG. 1. (Color online) Fitted spin-down R^- (a–c) and spin-up R^+ (d–f) reflectivities for the graded (black online) and uniform (red online) samples. The uncertainty-normalized difference in the data γ is shown along the bottom of each panel. Dashed lines in the γ plots correspond to ± 1. Measurements were taken in 750 mT for $T_A = 300\,^\circ$C (saturation, a, d), 820 mT for $T_A = 400\,^\circ$C (quasisaturation, b, e), and 1 mT for $T_A = 500\,^\circ$C (remanence, c, f). Error bars correspond to $\pm 1\,\sigma$.

sensitivity to Cu gradation in the samples, as evidenced by Fig. 1, which shows a comparison of PNR spectra for uniform and graded samples at fields corresponding to essentially flat regions of the hysteresis loop: a 750 mT saturating field for $T_A = 300\,^\circ$C, an 820 mT quasisaturating field (coming up from -850 mT) for $T_A = 400\,^\circ$C, and a remanent 1 mT field (after saturating offline in 1.6 T) for $T_A = 500\,^\circ$C. To better visualize the data at all Q_z, the fitted spin-down R^- (Figs. 1(a)–1(c)) and spin-up R^+ (Figs. 1(d)–1(f)) reflectivities are shown multiplied by $Q_z{}^4$ (the approximate reflectivity falloff for a perfect interface). Each Fig. 1 column corresponds to a different T_A and shows fitted data for the graded (R_G) and uniform (R_U) samples, with the residual difference in the data normalized by the experimental uncertainty $\gamma = \frac{R_G - R_U}{\sqrt{dR_G^2 + dR_U^2}}$, shown along the bottom of each panel. Normalized in this way, values of $|\gamma| > 1$ indicate statistically significant differences between graded and uniform samples. Figure 1 shows that the PNR spectra for the graded/uniform pairs become more similar at a high T_A—a clear indication that elevated T_A results in similar depth profiles for the two types of samples. This qualitative assessment is borne out by the models used to fit the data, which are shown in Fig. 2. Using fully dynamical calculations,[39,40] the data were well fit in terms of nuclear scattering length density $\rho(z)$ (Figs. 2(a)–2(c), indicative of the nuclear composition) and in-plane magnetization $M(z)$ (Figs. 2(d)–2(f)).[41] The magnetizations of the FePtCu films were assumed to vary linearly with distance from the SiO_2 interface z, whereas the cap magnetization was allowed to vary freely. The effects of Cu gradation are clearly manifested in the magnetic profiles (Figs. 2(d)–2(f)). For all three T_A,

the graded samples exhibit a clear reduction in magnetization with decreasing z, originating from a progressive reduction in the volume fraction of Fe as the Cu concentration is increased.[42] In stark contrast, the uniform reference samples show significantly flatter magnetization profiles, consistent with more uniform Cu profiles. T_A is observed to have a significant effect on the graded sample, because the $T_A = 300\,^\circ$C and $T_A = 400\,^\circ$C graded FePtCu films exhibit a roughly 25% decrease in magnetization from top to bottom, whereas the effect is $\sim$15% for the $T_A = 500\,^\circ$C film. So, as suggested by the data comparison in Fig. 1, model fitting confirms that the parts of the $T_A = 500\,^\circ$C graded/uniform pair have more similar magnetic profiles than do the lower T_A pairs. The overall decrease in the average magnetization, as T_A is increased, is consistent with a greater proportion of the film having transformed into the $L1_0$ phase.[43–45] Moreover, the best-fit models for all samples show a nonzero magnetization for the nominally Ta surface capping layer, implying some amount of vertical Fe diffusion for all T_A.

In addition, we have studied the field-dependent properties of the differently annealed samples using PNR and FORC techniques. Field-dependent PNR directly probes depth-dependent anisotropy variations, whereas FORC identifies switching events during the reversal process.

A. $T_A = 300\,^\circ$C

Model fitting of PNR data at varying fields (not shown) yields the magnetic profiles shown in Figs. 3(a) and 3(b). The in-plane magnetization depth profile $M(z)$, in absolute units, is
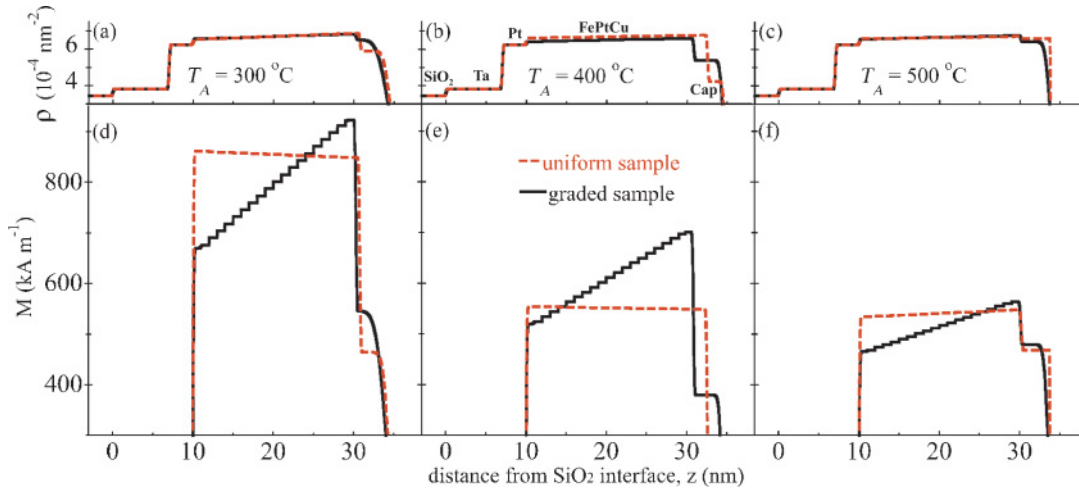
FIG. 2. (Color online) Nuclear (a–c) and magnetic (d–f) profiles used to fit the PNR data shown in Fig. 1.

shown in Fig. 3(a) as a function of applied field after negative saturation in −750 mT. To better distinguish depth variations in anisotropy from depth variations in total moment, the profiles in Fig. 3(a) are normalized by the positive saturation profile, as shown in Fig. 3(b). For a small positive field of 30 mT, the M/M_{sat} profile is essentially flat, because the sample is still nearly negatively saturated. However, as the applied field is increased, dramatic variations in the depth-dependent anisotropy start to become clear. The near surface, Cu-poor region of the FePtCu film approaches saturation ($M/M_{sat} = 1$) faster than does the Cu-rich bottom, and the Fe-infused Ta cap approaches saturation even faster than that. Clearly, the bottom of the film only approaches saturation in a relatively large field, because this Cu-rich region has preferentially transformed into the high anisotropy $L1_0$ phase. Thus, the sample exhibits a soft cap and a pronounced vertical anisotropy variation throughout the FePtCu film, as schematically represented in Fig. 3(c). These results also qualitatively agree with the magneto-optical Kerr effect on much thicker (50 nm) compositionally graded FePtCu films annealed at 300 °C, where the finite penetration depth of the laser showed the topmost ∼30 nm to be relatively soft.[21] Constraining the models to have a uniform anisotropy profile results in a significantly worse fit to the data.

Further insight into how the observed depth-dependent anisotropy variation affects the reversal mechanisms is carried out by analyzing the family of FORCs and the corresponding FORC distribution (calculated using Eq.(1)), shown in Figs. 4(a) and 4(b), respectively, for the graded FePtCu film annealed at 300 °C. The major loop, seen as the outer boundary of the FORCs, has a coercivity of 70 mT and exhibits a single sharp switching process. However, the FORC distribution (Fig. 4(b)), which reveals subtler information about the reversal, is characterized by two primary features: a peak located at $(H, H_R) = (10 \text{ mT}, -70 \text{ mT})$, indicated by a (red) dashed circle, and a negative–positive tail that extends downward parallel to the H_R axis, indicated by a (black) dashed oval. The peak not only locates, in (H, H_R) coordinates, the maximum irreversibility during switching but also reveals a great deal about the magnetic interactions present within the film. To

visualize this, the FORC that originates at $\mu_o H_R = -70$ mT is highlighted with a bold (red) line in Fig. 4(a) and a horizontal (red) dashed line in Fig. 4(b). We see that the highlighted FORC originates from a nearly demagnetized state near the coercive field, where a high degree of irreversible switching would be expected. More interestingly, as the applied field H is increased from $\mu_o H_R = -70$ mT, the highlighted FORC in Fig. 4(a) reaches positive saturation in a relatively small field, with a maximum slope at $\mu_o H = 10$ mT. If we consider the minor loop bounded by the descending branch of the major loop and the (red) highlighted FORC in Fig. 4(a), we clearly see it is significantly shifted toward negative applied fields. This behavior suggests the dominant soft phase components of the film are ferromagnetically exchange coupled to a higher anisotropy phase. Evidence of this higher anisotropy phase is found in the extended negative–positive tail in Fig. 4(b). This tail is generated by the irreversibility associated with switching the hardest components of the film, which require a more negative reversal field to fully switch. This feature, which extends to reversal fields of nearly $\mu_o H_R = -600$ mT, indicates that true saturation only occurs for very large negative reversal fields when the FORC diagram becomes featureless.[26] This high field saturation is also evident in the PNR data, which clearly show a nonsaturated profile at 120 mT (Fig. 3(b)). The high anisotropy contributions to the reversal also become apparent in the asymmetric FORC-SFD (Eq. (2)) and DCD-SFD (Eq. (3)) in Fig. 4(c), which both show an extended switching tail that extends toward large negative reversal fields. This asymmetry is consistent with the initial rapid switching of the dominant soft phase and gradual reversal of the hard phase components. From a qualitative fingerprinting standpoint, the FORC distribution and SFDs are strikingly similar to that of a previously studied polycrystalline FePt/FeNi hard/soft exchange spring bilayer.[27] In our graded FePtCu films, annealing at 300 °C has preferentially increased the $L1_0$ ordering of the Cu-rich portions near the bottom of the film, while most of the film remains in the low anisotropy A1 phase, thus creating a similar, although not as well defined, hard/soft bilayer structure, which is schematically
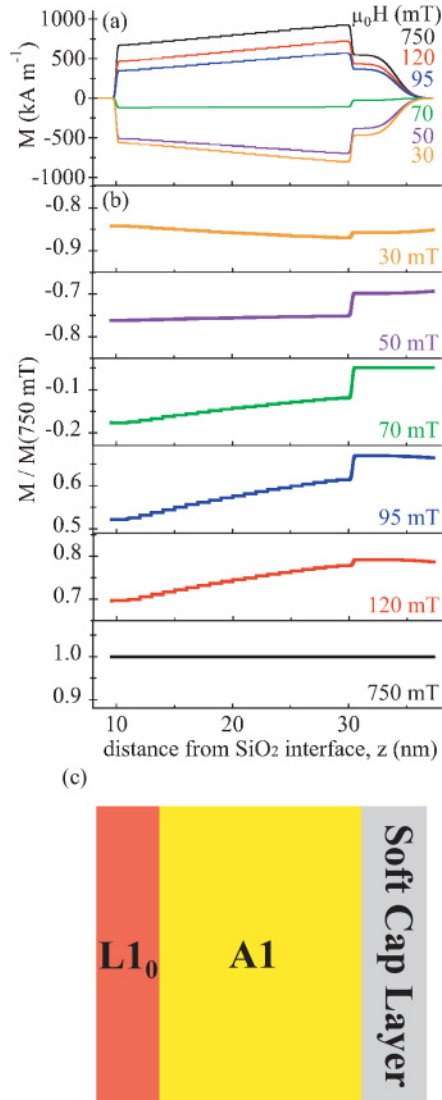
FIG. 3. (Color online) (a) Magnetization profiles used to fit the field-dependent PNR spectra for the graded sample annealed at $300\,^\circ$C. (b) Normalized magnetization profiles highlighting the anisotropy variation through the film thickness at the indicated fields after negative saturation in -750 mT. (c) Sample schematic highlighting the expected depth dependence of the phase profile.

FIG. 4. (Color online) Families of FORCs, FORC distributions, and SFDs for the graded (left) and uniform (right) FePtCu films annealed at $300\,^\circ$C. The first point of each reversal curve in (a) and (d) is shown by a black dot; the corresponding FORC distributions, shown as contour plots, are in (b) and (e), respectively. The horizontal (red) dashed line in (b) corresponds to the (red) bold FORC in (a), and the dashed (red) circle and dashed (black) oval highlight regions of the FORC diagram discussed in the text. The DCD-SFD as closed (black) squares and FORC-SFD as open (red) circles for the graded and uniform films are shown in (c) and (f), respectively.

represented in Fig. 3(c). We therefore conclude that $T_A = 300\,^\circ$C, although able to transform a portion of the film into the high anisotropy $L1_0$ phase, is not sufficient to establish an appropriate anisotropy gradient through the entire film thickness.

As a comparison, measurements on a compositionally uniform FePtCu film, also annealed at $300\,^\circ$C, are conducted (Figs. 4(d)–4(f)). The most obvious difference is that the uniform FePtCu sample has a much smaller coercivity, 24 mT, as compared to the graded FePtCu sample. This is expected, because $300\,^\circ$C is not sufficient to transform $(\mathrm{Fe_{53}Pt_{47}})_{85}\mathrm{Cu_{15}}$ into the high anisotropy $L1_0$ phase. In addition, differences in the reversal mechanisms become apparent when comparing FORC distributions of the graded and uniform samples (Figs. 4(b) and 4(e), respectively). Although both clearly
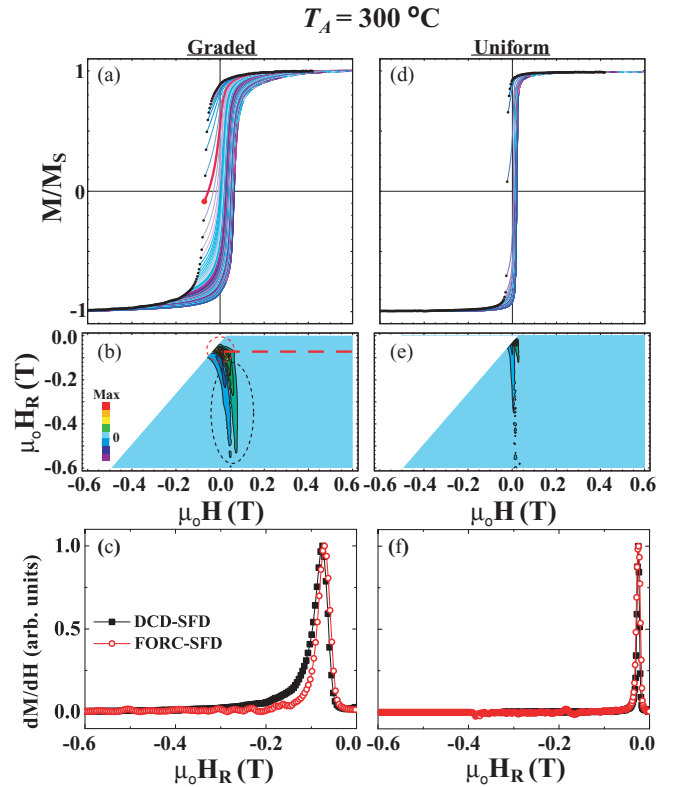
show a sharp irreversible peak, the prominent extended negative–positive tail found in the graded sample is mostly absent in the uniform film. Furthermore, the DCD-SFD and FORC-SFD (Fig. 4(f)) are symmetric and far narrower than the graded samples (Fig. 4(c)). These results indicate that this film primarily consists of a single highly uniform soft phase. However, the faint irreversible tail observed in the FORC distribution (Fig. 4(e)) reveals that even the nominally uniform film shows some small degree of anisotropy variation.

B. $T_A = 400\,^\circ$C

Interestingly, after annealing at $400\,^\circ$C, the variable field PNR measurements (measured after applying -820 mT), reveal a dramatically different anisotropy profile than what was observed for $T_A = 300\,^\circ$C. Figure 5 shows the absolute (a) and normalized (b) field-dependent magnetization depth profiles. The normalized profiles indicate that the surface region again approaches saturation faster than the FePtCu film, consistent with a soft, Fe-infused Ta cap. More striking however, is that the Cu-rich bottom of the FePtCu film approaches saturation in a smaller field than the Cu-deficient top—the opposite of
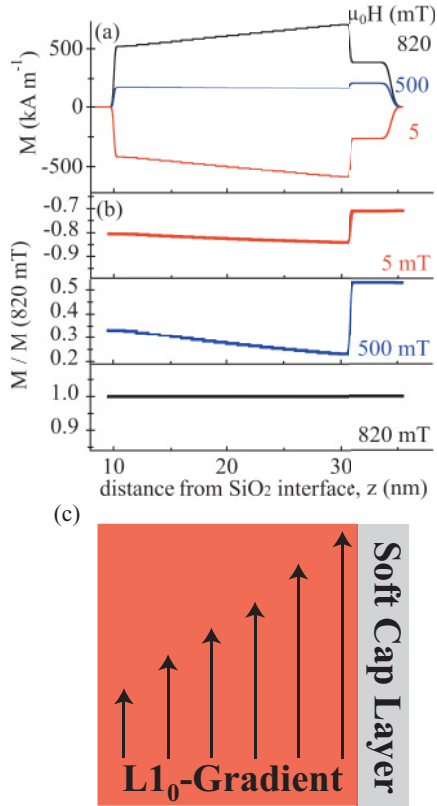
FIG. 5. (Color online) (a) Magnetization profiles used to fit the field-dependent PNR spectra for the graded sample annealed at $400\,^\circ$C. (b) Normalized magnetization profiles highlighting the anisotropy variation through the film thickness at the indicated fields after negative saturation in -820 mT. (c) Sample schematic highlighting the expected depth dependence of the phase profile, where the length of the black arrows represents the relative strength of the $L1_0$ phase at that particular depth.

FIG. 6. (Color online) Families of FORCs, FORC distributions, and SFDs for the graded (left) and uniform (right) FePtCu films annealed at $400\,^\circ$C. The first point of each reversal curve in (a) and (d) is shown by a black dot and the corresponding FORC distributions, shown as contour plots, are in (b) and (e), respectively. The horizontal (red) dashed lines in (b) and (e) correspond to the (red) bold FORCs in (a) and (d), respectively. The dashed black ovals in (b) and (e) and the brackets in (a) and (b) highlight regions discussed in the text. The DCD-SFD as closed (black) squares and FORC-SFD as open (red) circles for the graded and uniform films are shown in (c) and (f), respectively.

what was observed for the $T_A = 300\,^\circ$C sample. This inverted anisotropy profile has a simple explanation. At this elevated T_A, the total fraction of the film that is in the high anisotropy $L1_0$ phase has increased dramatically, as evident in the increased major loop coercivity of 548 mT (Fig. 6(a)). However, a significant compositional gradient still exists, as evident in Fig. 2(e). So, although the Cu-rich regions near the bottom of the film have undergone the A1 $\rightarrow$ $L1_0$ transformation at a lower T_A as compared to the rest of the film, the relative anisotropy strength is reduced because of the increased Cu content,[42] thus establishing a $L1_0$ gradient[45] through the bulk of the film thickness, which is now relatively soft toward the bottom, as schematically represented in Fig. 5(c).

Significant differences in the reversal mechanisms using the FORC technique are also observed after annealing at $400\,^\circ$C (Figs. 6(a)–6(c)). Two differences in the major loop (Fig. 6(a)) are immediately apparent from the sample annealed at $300\,^\circ$C. First, the coercivity has dramatically increased to 548 mT because of the overall increase in $L1_0$ ordering. Second, the shape of the major loop is markedly different. Instead of showing a single sharp reversal, a more gradual approach to saturation is observed and the reversal appears to occur in two stages. The FORC distribution (Fig. 6(b)) has also dramatically
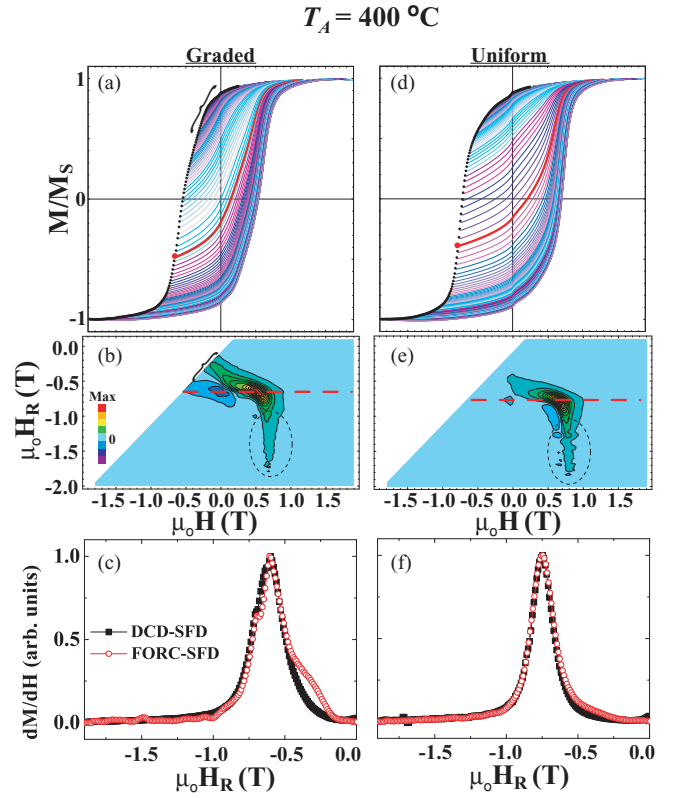
changed from the one observed for $T_A = 300\,^\circ$C (Fig. 4(b)), indicating a fundamentally different reversal mechanism. The FORC diagram is completely featureless for $\mu_o H_R \geqslant -150$ mT because of reversible switching processes. Then, for reversal fields of -550 mT $\leqslant H_R \leqslant -150$ mT, indicated with a bracket in Figs. 6(a) and 6(b), a low intensity ridge develops in the FORC diagram, marking the beginning of irreversible switching processes as the low anisotropy portions of the film begin to reverse. As the reversal field continues to decrease, the maximum irreversibility is found along $\mu_o H_R = -650$ mT, where a prominent negative–positive pair of peaks appears in the FORC diagram, indicated with a horizontal (red) dashed line in Fig. 6(b), and corresponds to the rapid irreversible switching of the film. As was similarly done in Fig. 4(a) for the sample annealed at $300\,^\circ$C, the FORC that corresponds to the maximum irreversibility, at $\mu_o H_R = -650$ mT, is highlighted with a bold (red) line in Fig. 6(a) to indicate the reversal path back toward positive saturation. Unlike the behavior exhibited in Fig. 4(a), the highlighted FORC in Fig. 6(a) gradually approaches positive saturation in a highly linear fashion and in a large applied field. This behavior is consistent with an

anisotropy gradient that has become better established through the film thickness at this T_A.

The FORC-SFD (Fig. 6(c)) is also fundamentally different from the sample annealed at 300 °C (Fig. 4(c)). Although both are highly asymmetric, the nature of the asymmetry is opposite for each sample. As the reversal field approaches more negative values, the sample annealed at 300 °C rapidly rises and then gradually decreases, whereas the sample annealed at 400 °C shows an initial gradual increase followed by a rapid fall. Because the anisotropy gradient has become better established after annealing at 400 °C, the reversal begins gradually as the low anisotropy layers slowly begin to reverse, in stark contrast to the sample annealed at 300 °C, which was dominated by the initial rapid switching of the dominant soft phase component. During the early stages of reversal, the DCD-SFD and FORC-SFD clearly differ (Fig. 6(c)), in that the FORC-SFD shows a significant shoulder that precedes the primary switching peak. This highlights the key difference between the two SFDs.[21] During the initial soft phase reversal, the remanent state changes little, which in turn renders it virtually invisible in the DCD-SFD. However, because the FORC-SFD is sensitive to the *irreversibility* associated with the soft phase reversal, it is able to clearly resolve the initial reversal stages. This shoulder in the FORC-SFD can be directly traced to the aforementioned low intensity ridge that developed in the FORC diagram for -550 mT $\leqslant \mu_o H_R \leqslant -150$ mT. Finally, as is also apparent in the FORC distribution, a faint tail, highlighted with a black dashed oval in Fig. 6(b), indicates the irreversibility associated with a residual hard phase component that is difficult to saturate.

Most significantly, the coercivity of the graded FePtCu sample, 548 mT, is considerably smaller than the uniform FePtCu reference sample, 730 mT, also annealed at 400 °C. This is expected, because a properly induced anisotropy gradient should result in a smaller switching field. The reversal mechanism of the uniform FePtCu sample is also markedly different. The (red) highlighted FORC in Fig. 6(d), which originates at $\mu_o H_R = -779$ mT and intersects the primary peak in the FORC distribution (Fig. 6(e)), approaches saturation differently than the graded sample (Fig. 6(a)). Whereas the graded sample is highly linear during much of its approach to saturation, the uniform sample is more concave. These subtle differences become clear in the FORC distributions. From a simple fingerprinting standpoint, the FORC distribution (Fig. 6(e)) indicates that the reversal mechanism of the uniform FePtCu sample is qualitatively similar to the uniform FePtCu sample annealed at 300 °C (Fig. 4(e)). Both show a single peak followed by a weak high anisotropy tail, indicated with a black dashed oval. In addition, both the DCD-SFD and the FORC-SFD (Fig. 6(f)) show a single highly symmetric peak and virtually overlap, as was also observed in Fig. 4(f). Interestingly, much like the uniform FePtCu sample annealed at 300 °C, the irreversible tail, indicated with the dashed black oval in Fig. 6(e), suggests that even a nominally uniform film contains some small degree of anisotropy variation.

C. $T_A = 500$ °C

After annealing the graded and uniform FePtCu films at 500 °C, the major loops (Figs. 7(a) and 7(d)), FORC
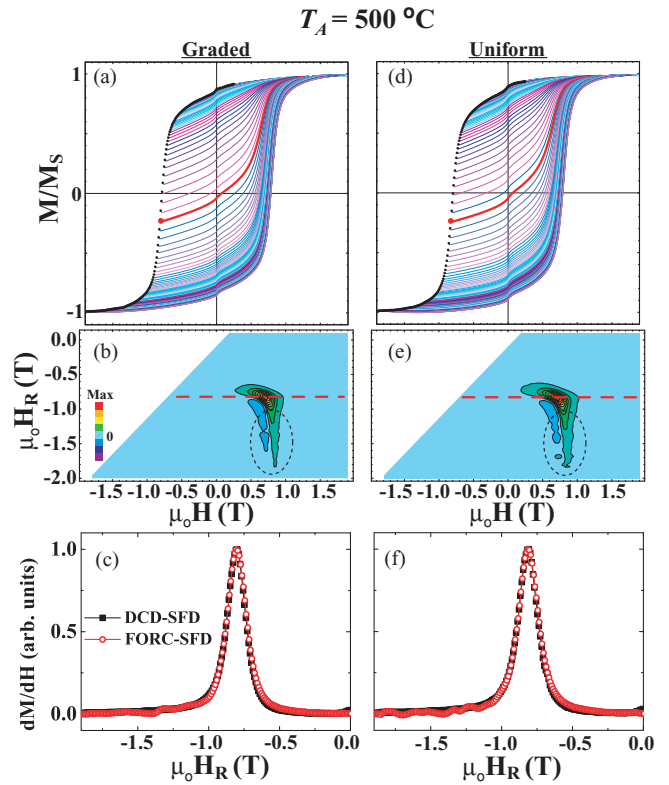

FIG. 7. (Color online) Families of FORCs, FORC distributions, and SFDs for the graded (left) and uniform (right) FePtCu films annealed at 500 °C. The first point of each reversal curve in (a) and (d) is shown by a black dot, and the corresponding FORC distributions, shown as contour plots, are in (b) and (e), respectively. The horizontal (red) dashed lines in (b) and (e) correspond to the (red) bold FORCs in (a) and (d), respectively. The dashed black ovals in (b) and (e) highlight regions of the FORC diagrams discussed in the text. The DCD-SFD as closed (black) squares and FORC-SFD as open (red) circles for the graded and uniform films are shown in (c) and (f), respectively.

distributions (Figs. 7(b) and 7(e)), and SFDs (Figs. 7(c) and 7(f)) become virtually indistinguishable. As discussed earlier, in regards to the PNR data, this suggests the Cu in the graded FePtCu sample has diffused throughout the film at this elevated T_A. It is also consistent that the graded and uniform samples should become identical, because both contain the same total Cu content. The coercivity of the major loop has further increased to 805 mT as the high anisotropy $L1_0$ phase has become better established and more uniformly distributed through the film thickness. The FORC distributions (Figs. 7(b) and 7(e)) show a single peak followed by an irreversible tail, indicating a reversal mechanism similar to that found in the uniform FePtCu samples annealed at 300 °C (Fig. 4(e)) and 400 °C (Fig. 6(e)). Furthermore, as was observed in the other uniform FePtCu samples, the DCD-SFD and the FORC-SFD (Figs. 7(c) and 7(f)) not only overlap but also are highly symmetric. Finally, the residual high anisotropy tail, indicated with a black dashed oval, is still present, possibly because of anisotropy variations from deposition fluctuations and/or temperature inhomogeneities during annealing.

IV. CONCLUSIONS

We conducted a detailed analysis of how the magnetic properties of both compositionally uniform and graded FePtCu films evolve as a function of T_A. PNR measurements show that Cu-graded FePtCu films exhibit significant depth-dependent magnetization variations for T_A of $300\,°\text{C}$ and $400\,°\text{C}$ that are consistent with the expected compositional gradient. After annealing at $500\,°\text{C}$, a drastic reduction in the slope of the magnetic profile is found for the graded sample that is consistent with interdiffusion of the Cu. In addition, all samples show a finite magnetization in the capping layer, most likely because of a fraction of Fe diffusing into the Ta. Furthermore, the field-dependent magnetization profiles clearly indicate depth-dependent magnetic anisotropy variations. Besides the very soft capping layer, the magnetic profile of the graded sample annealed at $300\,°\text{C}$ shows that the anisotropy gradient is not well established at this low T_A, because only the very bottom of the film has transformed into the hard $L1_0$ phase. The FORC analysis is consistent, indicating dominant soft phase switching with a significant hard phase component to the reversal. As the T_A is increased to $400\,°\text{C}$, dramatic changes to the anisotropy profile and reversal mechanisms are observed. Besides the magnetic soft capping layer, the field-dependent PNR measurements now indicate that the bottom of the film is comparatively soft. Although the increased T_A has transformed a larger portion of the film into the $L1_0$ phase, the significant Cu compositional gradient also decreases the relative anisotropy strength toward the bottom, Cu-rich region of the film. The FORC measurements confirm that the anisotropy gradient has become better established as the gradual reversal of the soft layers are found to facilitate the switching of the entire film. The switching field is indeed smaller than the uniform reference sample annealed at the same temperature. Finally, after annealing at $500\,°\text{C}$, the compositionally uniform and graded samples become virtually indistinguishable. This is consistent with the PNR results and suggests significant interdiffusion of the Cu in the compositionally graded FePtCu samples at this elevated temperature.

*randydumas@gmail.com

[1] J. Nogués and I. K. Schuller, J. Magn. Magn. Mater. **192**, 203 (1999).

[2] O. Hellwig, J. B. Kortright, K. Takano, and E. E. Fullerton, Phys. Rev. B **62**, 11694 (2000).

[3] E. F. Kneller and R. Hawig, IEEE Trans. Magn. **27**, 3588 (1991).

[4] D. Suess, Appl. Phys. Lett. **89**, 113105 (2006).

[5] D. Suess, J. Fidler, G. Zimanyi, T. Schrefl, and P. Visscher, Appl. Phys. Lett. **92**, 173111 (2008).

[6] K. Z. Gao and H. N. Bertram, IEEE Trans. Magn. **38**, 3675 (2002).

[7] J. P. Wang, Nat. Mater. **4**, 191 (2005).

[8] R. H. Victora and X. Shen, IEEE Trans. Magn. **41**, 537 (2005).

[9] T. W. McDaniel, J. Phys. Condens. Matter **17**, R315 (2005).

[10] J. G. Zhu, X. C. Zhu, and Y. H. Tang, IEEE. Trans. Magn. **44**, 125 (2008).

[11] M. H. Kryder and R. W. Gustafson, J. Magn. Magn. Mater. **287**, 449 (2005).

[12] H. J. Richter, IEEE Trans. Magn. **35**, 2790 (1999).

[13] J. Lee, V. Alexandrakis, M. Fuger, B. Dymerska, D. Suess, D. Niarchos, and J. Fidler, Appl. Phys. Lett. **98**, 222501 (2011).

[14] V. Alexandrakis, D. Niarchos, K. Mergia, J. Lee, J. Fidler, and I. Panagiotopoulos, J. Appl. Phys. **107**, 013903 (2010).

[15] J. S. Chen, L. S. Huang, J. F. Hu, G. Ju, and G. M. Chow, J. Phys. D: Appl. Phys. **43**, 185001 (2010).

[16] D. Goll, A. Breitling, L. Gu, P. A. van Aken, and W. Sigle, J. Appl. Phys. **104**, 083903 (2008).

[17] B. J. Kirby, J. E. Davies, K. Liu, S. M. Watson, G. T. Zimanyi, R. D. Shull, P. A. Kienzle, and J. A. Borchers, Phys. Rev. B **81**, 100405 (2010).

[18] B. J. Kirby, S. M. Watson, J. E. Davies, G. T. Zimanyi, K. Liu, R. D. Shull, and J. A. Borchers, J. Appl. Phys. **105**, 07C929 (2009).

[19] T. J. Zhou, B. C. Lim, and B. Liu, Appl. Phys. Lett. **94**, 152505 (2009).

[20] C. L. Zha, R. K. Dumas, Y. Y. Fang, V. Bonanni, J. Nogués, and J. Åkerman, Appl. Phys. Lett. **97**, 182504 (2010).

[21] V. Bonanni, Y. Y. Fang, R. K. Dumas, C. L. Zha, S. Bonetti, J. Nogués, and J. Åkerman, Appl. Phys. Lett. **97**, 202501 (2010).

[22] C. L. Zha, S. Bonetti, J. Persson, Y. Zhou, and J. Åkerman, J. Appl. Phys. **105**, 07E910 (2009).

[23] C. L. Zha, Y. Y. Fang, J. Nogués, and J. Åkerman, J. Appl. Phys. **106**, 053909 (2009).

[24] Y. Zhou, S. Bonetti, C. L. Zha, and J. Åkerman, New J. Phys. **11**, 103028 (2009).

[25] Y. Zhou, C. L. Zha, S. Bonetti, J. Persson, and J. Åkerman, Appl. Phys. Lett. **92**, 262508 (2008).

[26] J. E. Davies, O. Hellwig, E. E. Fullerton, G. Denbeaux, J. B. Kortright, and K. Liu, Phys. Rev. B **70**, 224434 (2004).

[27] J. E. Davies, O. Hellwig, E. E. Fullerton, J. S. Jiang, S. D. Bader, G. T. Zimanyi, and K. Liu, Appl. Phys. Lett. **86**, 262503 (2005).

[28] R. K. Dumas, C.-P. Li, I. V. Roshchin, I. K. Schuller, and K. Liu, Phys. Rev. B **75**, 134405 (2007).

[29] C. R. Pike, A. P. Roberts, and K. L. Verosub, J. Appl. Phys. **85**, 6660 (1999).

[30] R. K. Dumas, T. Gredig, C. P. Li, I. K. Schuller, and K. Liu, Phys. Rev. B **80**, 014416 (2009).

[31] R. K. Dumas, K. Liu, C. P. Li, I. V. Roshchin, and I. K. Schuller, Appl. Phys. Lett. **91**, 202501 (2007).

[32] J. E. Davies, J. Wu, C. Leighton, and K. Liu, Phys. Rev. B **72**, 134419 (2005).

[33] J. E. Davies, O. Hellwig, E. E. Fullerton, and K. Liu, Phys. Rev. B **77**, 014421 (2008).

[34] J.-W. Liao, R. K. Dumas, H.-C. Hou, Y.-C. Huang, W.-C. Tsai, L.-W. Wang, D.-S. Wang, M.-S. Lin, Y.-C. Wu, R.-Z. Chen, C.-H. Chiu, J. W. Lau, K. Liu, and C.-H. Lai, Phys. Rev. B **82**, 014423 (2010).

[35] M. T. Rahman, R. K. Dumas, N. Eibagi, N. N. Shams, Y.-C. Wu, K. Liu, and C.-H. Lai, Appl. Phys. Lett. **94**, 042507 (2009).

[36] J. Wong, P. Greene, R. K. Dumas, and K. Liu, Appl. Phys. Lett. **94**, 032504 (2009).

[37] C. L. Zha, J. Persson, S. Bonetti, Y. Y. Fang, and J. Åkerman, Appl. Phys. Lett. **94**, 163108 (2009).

[38] T. Maeda, T. Kai, A. Kikitsu, T. Nagase, and J.-I. Akiyama, Appl. Phys. Lett. **80**, 2147 (2002).

[39] C. F. Majkrzak, Physica B **221**, 342 (1996).

[40] C. F. Majkrzak, K. V. O'Donovan, and N. F. Berk, *Neutron Scattering from Magnetic Materials*. (Elsevier Science, New York, 2005).

[41] Although instrument resolution was insufficient to detect oscillations corresponding to 1 μm of SiO_2, this layer is assumed to be present in the model, and the resulting reflectivity calculations are sufficiently oversampled to prevent aliasing artifacts.

[42] M. L. Yan, Y. F. Xu, and D. J. Sellmyer, J. Appl. Phys. **99**, 08G903 (2006).

[43] Y. K. Takahashi, M. Ohnuma, and K. Hono, J. Magn. Magn. Mater **246**, 259 (2002).

[44] D. C. Berry and K. Barmak, J. Appl. Phys. **102**, 024912 (2007).

[45] Y. Y. Fang, R. K. Dumas, C. L. Zha, and J. Åkerman, IEEE Magn. Lett. **2**, 5500104 (2011).